Journal of Fluids and Structures 54 (2015) 235–246

Contents lists available at ScienceDirect

Journal of Fluids and Structures

journal homepage: www.elsevier.com/locate/jfs

Experimental study of the mean wake of a tidal stream rotor in a shallow turbulent flow

T. Stallard *, T. Feng, P.K. Stansby

School of Mechanical, Aerospace and Civil Engineering, University of Manchester, Manchester, M13 9PL, UK

ARTICLE INFO

Article history:
Received 30 June 2014
Accepted 19 October 2014
Available online 6 December 2014

Keywords:
Wakes
Channel turbulence
Shear layer
Tidal stream turbine

ABSTRACT

The mean wake of a three-bladed horizontal axis tidal stream turbine operating at maximum power coefficient has been investigated experimentally in a wide flume with width 11 times the depth, providing minimal restriction to transverse wake development and behaviour of large-scale horizontal turbulence structures. This is an important first stage for understanding wake interaction in turbine arrays and hence large-scale power generation. The rotor diameter has a typical value of 60% of the depth and the thrust coefficient is representative of a full-scale turbine. The shear layers originating from the rotor tip circumference show classic linear expansion downstream, with the rate of a plane shear layer vertically and 1.5 times that horizontally. These shear layers merge by around 2.5 diameters downstream forming a self-similar two-dimensional wake beyond eight diameters downstream with a virtual origin at two diameters downstream of the rotor plane. The spreading rate is somewhat less than that for solid bodies. The detailed velocity measurements made in the near wake show rotation and vorticity similar to that measured previously for wind and marine turbines although with asymmetry associated with bed and surface proximity. The longitudinal circulation in a transverse plane is conserved at about 1% of the swept circulation from the blade tip within two diameters downstream, the extent of detailed measurement. Turbines are usually designed using blade element momentum theory in which velocities at the rotor plane are characterised by axial and tangential induction factors and it is now possible to see how this idealisation relates to actual velocities. The axial induction factor corresponds to velocity deficits at 0.4–0.8 radii from the rotor axis across the near wake while the tangential induction factor at the rotor plane corresponds to velocities at 0.4–0.6 radii between 1–2 diameters downstream, indicating some general correspondence. For the two-dimensional self-similar far wake the two parameters defining the centreline velocity deficit and the transverse velocity profiles are likely to be insensitive to Reynolds number in turbulent conditions.

1. Introduction

Energy extracted from high velocity tidal flows by turbines is expected to make a significant contribution to electricity supply in many countries. We are here concerned with a three-bladed horizontal axis turbine which is the most common

* Corresponding author.
E-mail address: tim.stallard@manchester.ac.uk (T. Stallard).

http://dx.doi.org/10.1016/j.jfluidstructs.2014.10.017
0889-9746/

configuration, as it is for wind turbines. There have been many studies of power generation and thrust on marine and wind turbines both experimentally and numerically. Blade element momentum theory is a standard design tool for horizontal axis tidal turbines (Batten et al., 2008; Way and Collier, 2013). Design is determined by power output and the unsteady loading depends on the velocity and turbulence of the onset flow as well as the turbine operating conditions. For the anticipated large scale electricity generation by arrays of tidal turbines the onset flow to downstream turbines will be determined by the far wake of turbines located upstream. Here we undertake a laboratory study to investigate the mean far wake, and the upstream near-wake, of a representative tidal stream turbine at low blockage within a turbulent open channel flow.

The near wake has been modelled computationally, predicting time-averaged power and loading (e.g, McNaughton et al., 2014). Coherent tip vortices which break up downstream have been observed in LES (Large Eddy Simulation) studies (e.g. Afgan et al., 2013). Far field velocities due to a porous disc turbine representation have been measured by Myers and Bahaj (2010) and due to model turbines by Maganga et al. (2010) with low blockage; they both showed that increasing upstream turbulence increased wake recovery, but the resulting mean flow was not categorised. Chamorro et al. (2013) investigated the effect of upstream turbulence on turbine response and its effect on wake recovery. Response was coupled to upstream turbulence below a critical rotation frequency and uncoupled at higher frequencies. Wake recovery was linked to the large scale motions in the flow resulting from the tip vortices. There have been many more studies of wind turbine wakes (e.g. Vermeer et al., 2003) which relate directly. These include computational studies (e.g. Wu and Porte-Agel, 2011), field trials (Högstrom et al., 1988; Magnusson and Smedman, 1999) and experimental laboratory studies, typically at small geometric scale with reduced thrust coefficient (Hu et al., 2011; Zhang et al., 2012). These show the importance of upstream turbulence in enhancing wake recovery which is generally more significant than shear effects. Various wake details have been analysed including tip vortex generation and breakdown and large scale wake meandering. An important difference for tidal turbines is that the wake is constrained vertically by a water (free) surface which is particularly likely to influence the far wake. It is well known that the turbulence structure of such shallow flows is anisotropic with horizontal length scales many times the vertical (e.g. field measurements of Thomson et al. (2012) and inferred from modelling by Stansby (2003)). This could also be a limitation for the study of Chamorro et al. (2013) where the streamwise length scale was 1.4 times the depth and both the horizontal structures and the far wake could be influenced by the channel width of 2.4 times the depth.

In this study we investigate the near and far wake in a wide flume with width more than 10 times the depth so that horizontal turbulence and far wake will not be significantly influenced by the side walls. We are concerned with the mean flow characteristics and how the relatively unconstrained, and nearly axisymmetric, near wake merges into the depth-constrained far wake. The turbine diameter is about 60% of the water depth and the turbine operates at maximum efficiency, at the tip speed ratio for maximum power coefficient for this geometric scale. The rotor is designed such that the thrust coefficient is typical of a full-scale turbine. Since the blade element momentum theory is a standard design tool based on axial induction and tangential induction factors we relate the values resulting from this rotor design to the physical wake.

The paper is organised as follows: Section 2 Experimental Arrangement, Section 3 Wake Velocity Deficit, Section 4 Near Wake Rotation, Section 5 Wake Turbulence and Section 6 Conclusions.

2. Experimental arrangement

Measurements were made of the wake generated downstream of a single turbine of diameter $D=0.27$ m located at mid-depth in an open channel flow of width $W=5$ m, depth $h=0.45$ m and with mean velocity $U_0=0.46$ m/s. The longitudinal, vertical and transverse axes are denoted as x, z and y. The global blockage based on swept area to channel cross section (A_D/Wh) is therefore 2.5% and wake expansion is effectively unconstrained in the transverse direction with $W=18.5D$, but is constrained vertically by the bed and free-surface as $h=1.67D$. The locations (X, Y, Z) reported herein are relative to the rotor origin located at $x_0=13.3h$ from the flume inlet. Some further details on this arrangement, including a schematic of the flume, are given by Stallard et al. (2013). A 3-bladed rotor is employed as a likely form of rotor for widespread deployment in large farms. Horizontal thrust, applied torque and rotational speed of the rotor were recorded.

2.1. Flow velocity measurement

Time varying velocities were measured using a NORTEK Vectrino+ ADV with velocity range ± 1 m/s, sample volume dimension of 3 mm and transmit length of 8.7 mm (Nortek, 2006). Three components of velocity were recorded, u_x, u_y, u_z. The probe was positioned in a vertical $y-z$ plane downstream of the rotor using an automated traversing system with position accurate to less than 1 mm. Signal to noise ratio (SNR) and correlation coefficient (COR) tested prior to each set of measurements indicate that the majority of samples ($>95\%$) have SNR >15 dB and COR $>90\%$. At each co-ordinate a 60 s sample was recorded at 200 Hz. This provides resolution into the turbulence subrange (frequency 32 Hz based on channel flow velocity, see p. 30 Nezu and Nakagawa, 1993) and was found to be sufficient for time-averaged values of velocity, denoted U, and of longitudinal turbulence intensity (u'_x/U_0 where u'_x is the rms of fluctuating longitudinal velocity) to be calculated to within 2% and for turbulence length scales to be converged to within 5%.

2.2. Incident flow

A constant flow-rate was obtained by pumps located between 2.5 m deep basins at either end of a 12.5 m long, flat horizontal bed. The base and walls of the flume were Perspex panels. A vertical porous plate was located across the inflow ($y-z$ plane) comprising a triangular array of 12 mm diameter holes at 15 mm centre-to-centre pitch in 3 mm thick stainless steel. This removed the large scale eddies from the end basin resulting in nearly spatially uniform anisotropic turbulence at the test section typical of a wide channel. The mean longitudinal velocity was $U_0 = 0.463$ m/s. Froude number was thus 0.22 and channel Reynolds number $Re_h = U_0 h/\nu = 2.1 \times 10^5$. For $z < 0.3h$ the profile of longitudinal velocity reduces to Eq. (1) with friction velocity $U^* = 0.0167$ m/s and where κ is the von Karman constant of 0.41 and C is 5. The mean velocity profile is shown in Fig. 1(a)

$$\frac{U(z)}{U^*} = \frac{1}{\kappa}\log\left(\frac{zU^*}{\nu}\right) + C. \tag{1}$$

Turbulence intensity is nearly constant across the water depth at cross sections just upstream and downstream of the rotor plane as shown in Fig. 1(b). Average longitudinal turbulence intensity is 12% at the rotor plane ($X=0$) but decays to 10% (approximately) over a distance of 10D. The total turbulence intensity ($u'/U_0 = [(3U_0)^{-1}\sum_{i=1}^{3}(u_i')^2]^{1/2}$) is also shown in Fig. 1 (b) but hereafter turbulence intensity implies longitudinal only. The integral length scales of the ambient turbulence measured by a two point cross correlation method (by Eq. (2) from Pope, 2000) at mid-depth are $L_{x,x}, L_{y,y}, L_{z,z} = 0.56h, 0.33h$ and $0.25h$. Sample duration was 900 s for these measurements. The transverse length scale is thus slightly greater than the vertical and the longitudinal about twice and is a little greater than half the depth. It is well known that horizontal scales are greater than vertical in shallow flows but also vary widely (e.g. Thomson et al., 2012). These values may only be considered representative of field data and this study is concerned with time-averaged velocity and turbulence intensity.

$$L_{i,j} = \int_0^\infty R_{ij}(r)\,dr, \quad R_{ij}(r) = \frac{\langle \overline{u_i(r)}\,\overline{u_j(r+dr)} \rangle}{\langle \overline{u_i^2} \rangle}, \tag{2}$$

where dr is the separation between velocity measurement points on the axis $i, j = x, y$ or z.

2.3. Rotor design

A 3-bladed rotor was developed to generate a wake that is representative of the momentum extraction and swirl generated by a full-scale turbine as described by Whelan and Stallard (2011). At three-quarter span and tip speed ratio of 4.5, chord Reynolds number was $Re_C \approx 30\,000$ compared to $Re_C > 6 \times 10^6$ for a full-scale rotor of 18 m diameter. Maximum lift to drag ratio for a foil section at Re_C less than 50 000 is around 15 compared to around 200 for a full-scale rotor (Lissamen, 1983) and this limits the torque developed for a given thrust. Each blade thus comprised a Göttingen 804 foil with radial variation of chord length and twist angle selected to (i) attain thrust coefficient equivalent to a full-scale turbine over a range of tip speed ratios and (ii) attain similar peak power coefficient despite the moderate chord Reynolds number of the experiment. On this basis the blade geometry listed in Table 1 was selected using a blade element code with

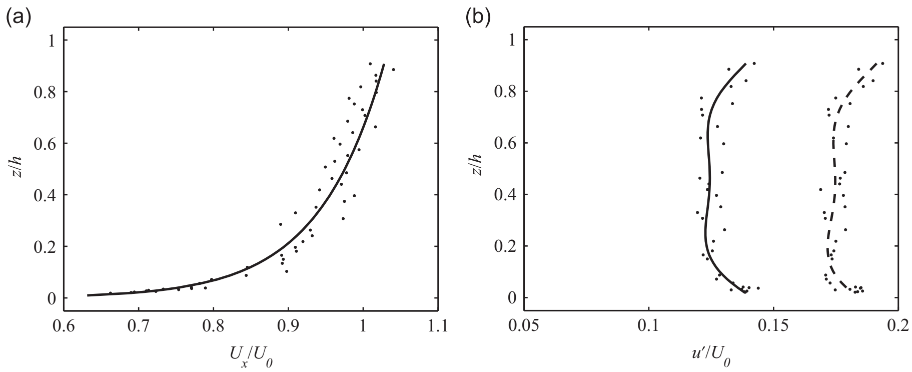

Fig. 1. Depth profile of velocity and turbulence intensity at rotor plane. (a) Longitudinal velocity. (b) Turbulence intensity of longitudinal velocity u_x'/U_0 (solid) and total velocity u'/U_0 (dashed).

Table 1
Radial variation of chord length and angle relative to rotor plane.

r/R	0.111	0.241	0.333	0.48	0.537	0.630	0.733	0.833	0.925	0.998
c/R	0.111	0.148	0.222	0.204	0.185	0.165	0.144	0.130	0.115	0.096
θ○	38	23	16	11.3	9.0	7.5	5.8	4.1	3.1	2.6

Table 2
Lift and drag coefficients for Göttingen 804 section Hassan (1993).

For $-30^\circ \le \alpha \le 10^\circ$												
α	-30	-20	-10	-7	-6	0	1	2	4	8	9	10
C_L	-0.70	-0.50	-0.30	-0.40	-0.51	0.24	0.37	0.49	0.74	1.24	1.19	1.11
C_D	0.48	0.25	0.13	0.12	0.11	0.06	0.06	0.06	0.06	0.10	0.12	0.14
For $10^\circ < \alpha \le 50^\circ$												
α	12	14	16	18	20	25	30	35	40	45	50	
CL	0.97	0.91	0.89	0.91	0.94	1.06	1.16	1.19	1.16	1.11	1.10	
CD	0.23	0.29	0.35	0.41	0.46	0.59	0.74	0.89	1.01	1.07	1.07	

lift and drag coefficients for this foil section for $Re_C = 20\,000$ (Miley, 1982) and 30 000 (Hassan, 1993) (Table 2). The 3-bladed 0.27 m diameter rotor was manufactured in one piece by the rapid prototyping method Synthetic Laser Sintering (SLS) using 0.2 mm thick layers of glass fibre reinforced polymer acrylic.

2.4. Mechanical system

The rotor was mounted directly on the shaft of a 90° bevel gearbox with acrylic gears (Huco B332.31.3). The gearbox was supported by a 15 mm outer diameter stainless steel rod with strain gauges located 800 mm above the rotor axis. A 4 mm diameter driveshaft transferred mechanical torque to an encoder and motor located above the water level. Only the rotor, gearbox and lower part of the supporting shaft were immersed. The centreline of the supporting shaft was located 0.15D downstream of the rotor plane and the gearbox extended to 0.2D downstream. This configuration was employed to minimise dimensions of the immersed support structure and allowed measurement of flow velocity to within 0.4D downstream of the rotor plane.

Thrust was measured by a full-bridge strain gauge (EA-06-125PC-350W by Micro Measurements) connected to a National Instruments SCC-SG24 strain gauge module. Strain gauges were mounted on the support shaft 800 mm above the rotor axis and calibrated by measurement of the voltage corresponding to fixed increments of load applied to the hub prior to immersion. A linear relationship was obtained between applied load and measured voltage by least-squares-best-fit. The residual was less than 0.1% in all cases. Horizontal force measured by the strain gauges is due to horizontal thrust on the swept area of the rotor (F_x) and drag on the supporting structure (F_{tower}). Measurements of the force on the support structure only, i.e. without the rotor attached, indicates an average force, $F_{\text{tower}} = 0.26$ N . In comparison, thrust on the rotor plane was approximately $F_x \sim 6$ N indicating that support structure loading was an order of magnitude smaller than the rotor thrust. The thrust coefficients reported herein were obtained after subtracting the nominal tower load: $C_T = 2F_x/\rho A_D U_0^2$.

Angular displacement was measured using a HEDS 9000 quadrature encoder reading an HEDM 6120 T12 code wheel. The code-wheel has 2000 counts per revolution thus providing position resolution of $\pi/100$. Angular speed, ω_m, was obtained by differentiation of the measured angular displacement. Torque applied to the rotor was defined by a dynamometer system developed by Brown (2009) and described by Weller et al. (2010). This comprised a firmware controller that specifies the bridge current I_A across a CROUZET 82800 series 24 V DC motor as a function of measured angular speed. The net retarding torque, Q, is the sum of mechanical friction and motor torque. The mechanical friction was defined by the motor torque that maintains constant angular speed without rotor attached.

2.5. Rotor performance

The operation of a tidal stream turbine is typically characterised by the variation of thrust coefficient and power coefficient with tip speed ratio ($\beta = \omega_m R/U_0$ where R is rotor radius). Measured thrust coefficient ($C_T = 2F_x/\rho U_0^2 A_D$) and power coefficient ($C_P = 2Q\omega_m/\rho U_0^3 A_D$) are in reasonable agreement with predictions obtained from a blade element method (Bossanyi, 2009) over the range $3 < \beta < 7$ as shown in Fig. 2. For all wake studies reported herein, mechanical torque was specified to obtain a mean tip speed ratio of $\beta = 4.5$, close to maximum C_P. At this operating point predicted C_T is equal to that of a full-scale turbine whereas predicted $C_P = 0.33$ compared to 0.46 for a full-scale turbine. For each wake traverse, the time-averaged thrust and tip speed ratio varied by less than 5%.

3. Wake velocity deficit

Velocity was measured downstream of the rotor plane on a Cartesian grid of points in the vertical $y-z$ plane ($dy = dz = 20$ mm) at four x-coordinates $X = 0.5D, 1D, 1.5D$ and $2D$ and along horizontal and vertical lines normal to and through the rotor centreline over the range $1.5D < X < 12D$. Velocity measurements were also taken along the axial centreline to 20D downstream. Vertical plane measurements provide insight into the initial wake structure and development while the transverse, vertical and longitudinal velocity variations provide insight into far-field wake development with the influence of bounding surfaces.

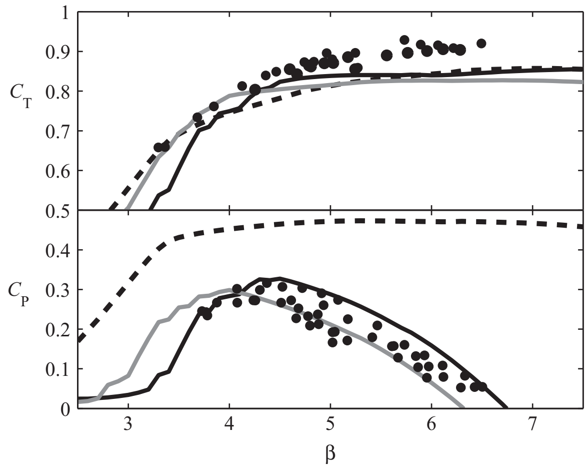

Fig. 2. Variation of thrust coefficient C_T and power coefficient C_P with Tip Speed Ratio β for geometry of Table 1 obtained by blade element code with foil performance from Miley (1982) (solid black line) and Hassan (1993) (sold grey line) and experimental measurement (solid points). Predicted coefficients for representative full-scale turbine also shown (dashed). All predictions for unbounded flow.

3.1. Overview of wake structure

The deficit of mean velocity along the centreline of the wake was found to be $\Delta U = 0.9U_0$ at 1D downstream of the rotor but velocity recovers to within $0.2U_0$ by 10D downstream. Within this distance, longitudinal turbulence intensity is between 10 to 15% with the maximum occurring 3D downstream. Over the range 10D to 20D further recovery of mean velocity is gradual with a deficit of $0.12U_0$ observed at 20D. This longitudinal variation is consistent with previous measurements for wind and marine turbines.

The transverse profiles of longitudinal velocity shown in Fig. 3 are approximately symmetric and follow a nearly Gaussian profile. A small bypass flow with velocity greater than ambient velocity is evident just outside the rotor swept area at 1.5D and 2D but beyond 4D only a velocity deficit is observed. The maximum velocity deficit occurs close to the rotor axis and is $0.8U_0$ and $0.5U_0$ at 2D and 4D downstream respectively. Over the same longitudinal distance the extent over which a deficit occurs expands transversely from 1.5D to 2.0D approximately. In contrast to the symmetric transverse profiles, the vertical profiles are asymmetric about the centreline beyond 2D downstream as shown in Fig. 3. At 1.5D downstream the vertical profile is nearly symmetric but the maximum deficit is above the centreline. This extends over the range 2D to 6D.

In this channel, with aspect ratio of 11.1:1, the rotor wake was effectively unconstrained in the transverse direction but constrained in the vertical direction due to the proximity of both the channel bed and free surface, both at distance 0.83D from the rotor axis. For $X > 6D$ downstream the vertical velocity profile is similar to a channel velocity profile and wake expansion occurs in the transverse direction only. Immediately downstream of the rotor a bypass flow occurs around the turbine. These two regions of the wake are analysed in the following sections.

3.2. Far wake

The velocity profiles of a free shear layer can be expressed in a self-similar form. In general, for an axisymmetric wake, the self-similar form follows a Gaussian profile (Pope, 2000, p. 148):

$$\frac{\Delta U}{\Delta U_{max}} = \exp\left(-\ln(2)\frac{y^2}{y_{1/2}^2}\right), \tag{3}$$

where $\Delta U = U_0 - U_x$ denotes the local velocity deficit, ΔU_{max} is the maximum velocity deficit and $y_{1/2}$ is the half-width, the distance from the centreline at which the velocity deficit is half of maximum. A wake is considered to be self-similar when the spreading-rate S is constant with downstream distance x:

$$S = \frac{U_0}{\Delta U_{max}}\frac{dy_{1/2}}{dx}. \tag{4}$$

Since ambient velocity U_0 is constant, the half-width $y_{1/2}(x)$ must be proportional to a power of x with an exponent exactly unity higher than that for the maximum deficit $\Delta U_{max}(x)$. Previous investigators have reported the relations $\Delta U_{max} \propto x^{-1/2}$ and $y_{1/2} \propto x^{1/2}$ for plane wakes and $\Delta U_{max} \propto x^{-2/3}$ and $y_{1/2} \propto x^{1/3}$ for axisymmetric wakes. Wakes generated by different obstacles develop different self-similar spreading rates. Spreading rates for unbounded plane wakes downstream of a flat plate, circular cylinder and airfoil are S=0.073, 0.083 and 0.103 (Pope, 2000, p. 149). It is evident from Fig. 3 that a Gaussian form does not describe the vertical profiles and does not describe transverse profiles within 2D downstream of the rotor where a bypass flow is observed. However Eq. (3) is found to be representative of the transverse profile at

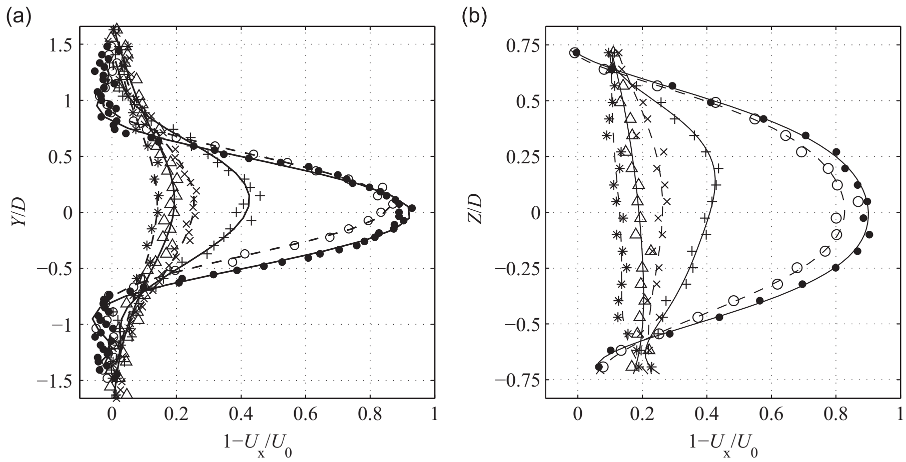

Fig. 3. Transverse and vertical profiles of velocity deficit at $X=1.5D$ (●), $2D$ (○), $4D$ (+), $6D$ (×), $8D$ (Δ) and $12D$ (∗). Curves indicate trend only. Mean thrust and tip speed ratio over all samples, $C_T=0.85\pm4.5\%$ and $\beta=4.6\pm3.5\%$.

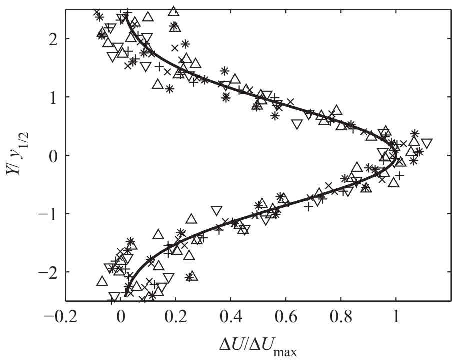

Fig. 4. Transverse profile of velocity deficit at sections $4D<X<12D$ (symbols as Fig. 3) compared to Eq. (3) (solid curve).

distances $X\geq 8D$ (Fig. 4). The corresponding maximum deficit $\Delta U_{\max}$ and transverse half width $y_{1/2}$ are plotted in Fig. 5. For $X\geq 8D$ the rate of recovery of velocity and expansion of half-width follow those observed for a plane wake:

$$\frac{\Delta U_{max}}{U_0}=0.864(x/D)^{-1/2}-0.126, \tag{5}$$

$$\frac{y_{1/2}}{R}=0.412(x/D)^{1/2}+0.500. \tag{6}$$

The transverse spreading parameter (Eq. (4)) is thus 0.03; smaller than spreading rates observed for plane bluff bodies in unbounded flows.

3.3. Near wake

At one diameter downstream the transverse profile of axial velocity, $U_x(Y)$, is nearly axisymmetric across the swept area of the rotor with a maximum deficit of $0.9U_0$ occurring near the rotor centreline as shown in Fig. 6. The location of the maximum deficit is slightly offset from the rotor axis in both the transverse and vertical directions. This can be attributed to the rotation of a reduced velocity region which develops downstream of the tower and is rotated within the wake (described in Section 4). The tower wake is clearly observed $0.5D$ downstream of the rotor plane both directly above the rotor and within the upper part of the swept area but this and the nacelle wake have dissipated by $1D$. At both these downstream planes, the radial gradient of velocity is nearly uniform over the swept area and a narrow shear layer is observed at the boundary to the ambient flow. This layer expands rapidly with downstream distance and is narrower in the vertical direction than the transverse direction. Further downstream a similar structure is maintained as the deficit reduces and velocity gradient decays up to $2D$.

According to linear momentum theory, the velocity across the rotor plane (i.e. at $X=0$) is defined by the axial induction factor, a, as $U_x(X=0)=(1-a)U_0$. A blade element momentum theory calculation is limited to within the rotor radius, and

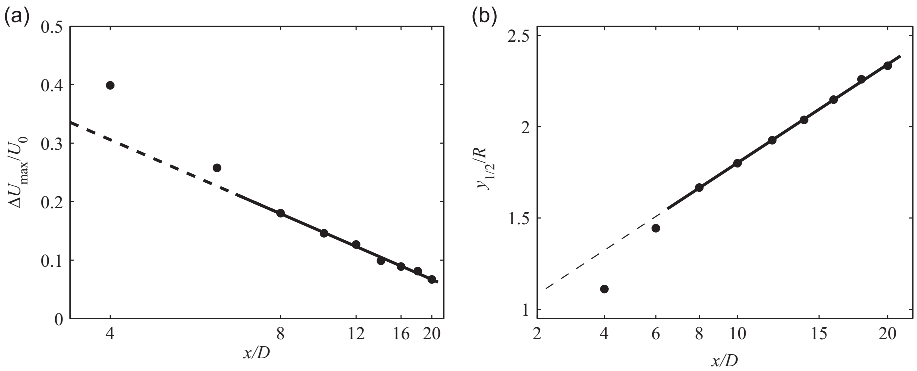

Fig. 5. Velocity deficit and half-width of self-similar wake profiles corresponding to Fig. 4 (●) and Eqs. (5) and 6 over the best-fit range (solid curve) and extrapolated (dashed curve).

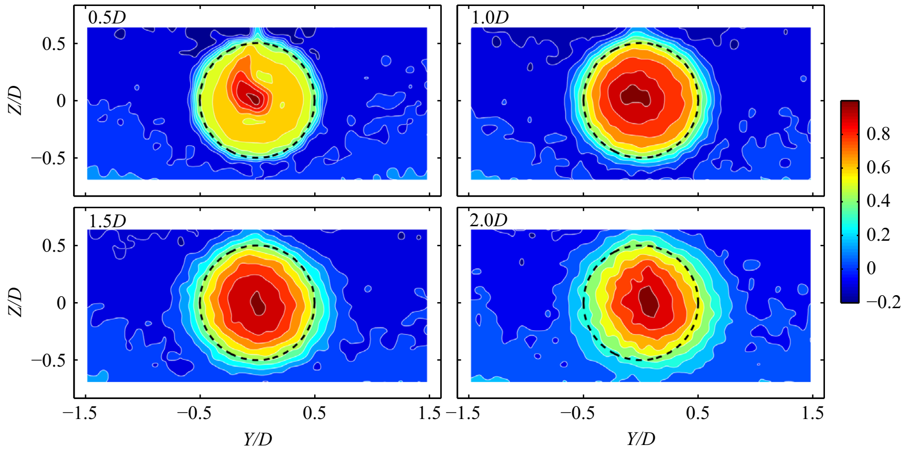

Fig. 6. Velocity deficit $(1-U_x/U_0)$ at sections $0.5D, 1D, 1.5D$ and $2D$ downstream of rotor. Each contour plot obtained from 60 s average from 780 co-ordinates in the $y-z$ plane. Mean thrust and tip speed ratio over all samples, $C_T = 0.88 \pm 5\%$ and $\beta = 4.7 \pm 3.5\%$.

correction factors are typically applied near the blade root and tip. However, it is useful to assess the suitability of this approach for predicting the initial velocity deficit and this is shown in Fig. 7. As expected, the high axial induction factor predicted near the tip is not observed in the measurements at $X = 0.5D$. The model only slightly underpredicts the velocity deficit at $X = 0.5D$ and $1D$ over the range $0.3 < r/R < 0.9$.

An axisymmetric wake can be considered as a shear layer of width δ centred about a radius r_δ. Various definitions of shear layer width have been employed to characterise axisymmetric shear layers (e.g. Hussain and Zedan (1978)). Here, the approach of Brown and Roshko (1974) is followed and the shear layer width is defined by Eq. (7) as a function of the ambient flow velocity and the maximum velocity gradient across the shear layer. The radius to this maximum gradient r_δ denotes the centreline of the shear layer. This is employed in preference to the half-width or momentum width since velocity deficit varies azimuthally and the flow is constrained vertically.

$$\delta = U_0 \frac{dU}{dr}\bigg|_{max}^{-1} \tag{7}$$

The radial gradient of velocity is obtained by a least-squares best-fit of a polynomial for velocity at radial increments $dr = 40$ mm obtained by interpolation from the measurements on a Cartesian grid. Immediately downstream of the rotor plane ($X = 0.5D$), the shear layer width is non-uniform about the circumference with vertical width of approximately $0.18D$ compared to transverse width of approximately $0.36D$ as shown in Fig. 8. This is due to the bypass flow above and below the rotor. Further downstream the shear layer width becomes more uniform but width in the vertical direction remains smaller than in the transverse direction. The shear layer width increases linearly with downstream distance as shown in Fig. 8(e). The vertical expansion rate is $d\delta/dx = 0.22$ and this is similar to rates observed by Brown and Roshko (1974) for an unconfined plane jet with comparable Reynolds number and initial deficit. The transverse expansion rate is linear over the range $1D$ to $2.0D$ and is approximately 1.5 times that in the vertical direction ($d\delta/dx = 0.33$).

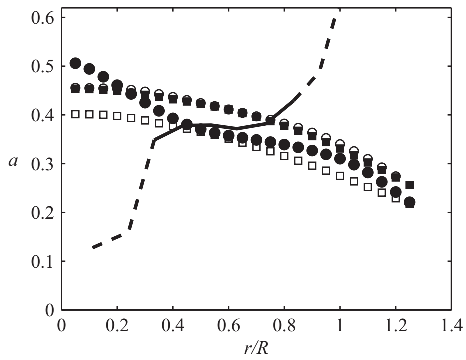

Fig. 7. Radial variation of axial induction factor from measurements at 0.5D (●), 1D (○), 1.5D (■), 2D (□) and by Blade Element Momentum Theory (–).

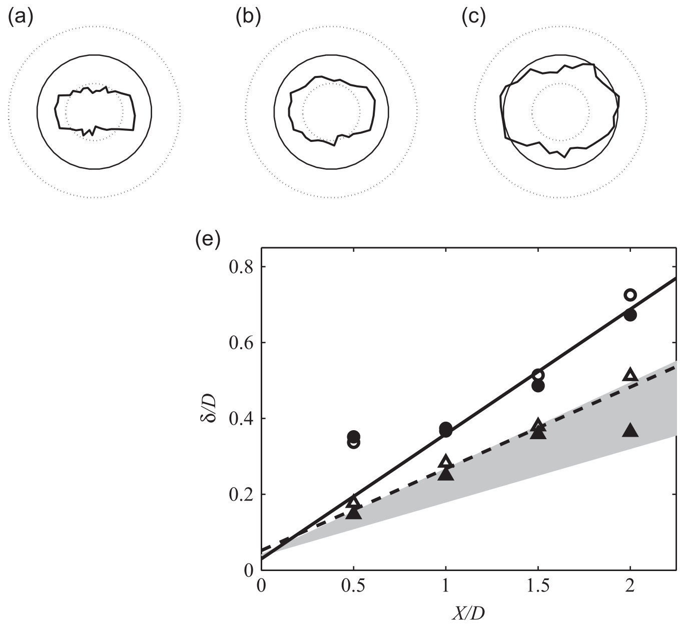

Fig. 8. Shear layer width δ by Eq. (7) (thick solid curve). (a)–(d) Azimuthal variation over transverse planes at $X = 0.5D$ to $2D$ relative to a rotor radius R (thin solid curve) and to $(1 \pm 0.5)R$ (dotted curve). (e) Longitudinal variation in transverse (○, from $U_x(Y)$ at $Z = 0$) and vertical (Δ from $U_x(Z)$ at $Y = 0$) directions. Shaded region denotes $d\delta/dx$ range 0.145 to 0.22 (Brown and Roshko, 1974). (a) 0.5D. (b) 1D. (c) 1.5D. (d) 2D. (e) Longitudinal variation.

At 0.5D downstream, the radius at which maximum gradient occurs (the shear layer centreline) forms a slightly elliptic profile as seen in Fig. 9. Over the range 0.5D to 2D the shear layer radius reduces slightly but is similar to the rotor radius. There is some evidence of depth constraint at 1.5D downstream where the shear layer is parallel to the bed beneath the wake. The greater transverse expansion rate causes the shear layers to interact at the centre of the wake by around 2.5D downstream. Further downstream the radius to the shear layer centreline in the transverse direction is consistent with the half-width variation previously identified for a self-similar transverse profile (Fig. 9(e)) increasing from the rotor radius at $X = 2.0D$.

4. Near wake rotation

Although the near wake is not exactly axisymmetric, it is informative to consider velocity components in a polar frame rather than Cartesian frame. Radial (U_r) and azimuthal velocity (U_θ) relative to the axis of the rotor are shown in Fig. 10. Rotation is observed within the wake over the range $0.5D \le X \le 2D$. This develops from a band of high azimuthal velocity at radius $0.3R < r < 0.7R$ at 0.5D to nearly uniform rotation over the range $0.2R < r < 0.9R$ at 1D. The rotating region expands outwards and the centre of rotation shifts slightly upwards with downstream distance. Less than 1D downstream, the surrounding flow is similar to the ambient flow. With increasing distance downstream entrainment of the surrounding flow is observed. At 1D this is over one quarter of the circumference and extends over three-quarters of the circumference by 2D. The flow on either side of the rotor changes its direction from divergent to convergent into the rotor wake core. This indicates that the process of mass and momentum mixing between turbine wake and the surrounding flow starts after 1D

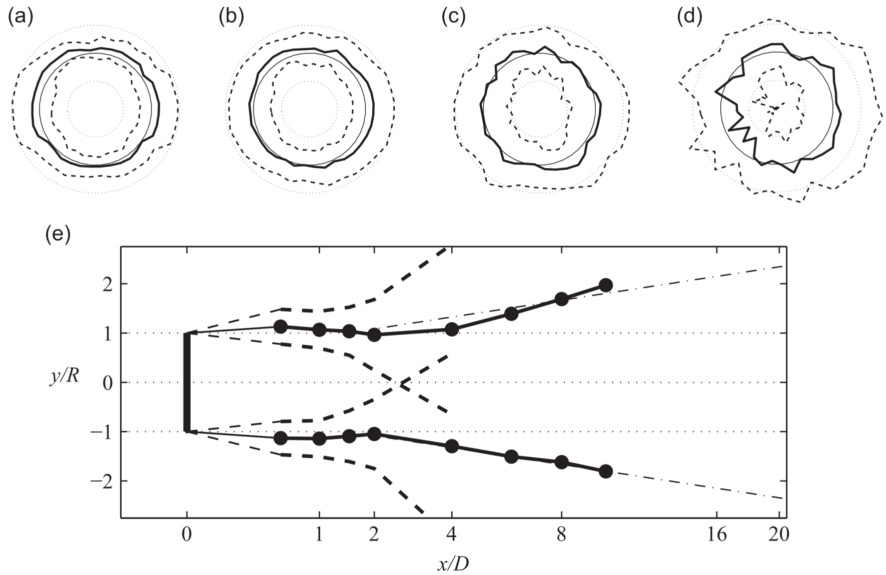

Fig. 9. Shear layer radius, r_δ (thick curve), and extent, $r_\delta \pm \delta$ (thick dashed) from velocity profiles at $X=0.5D$ to $10D$ (●). (a) to (d): azimuthal variation over transverse planes at $X=0.5D$ to $2D$ relative to rotor radius R (thin curve) and to $(1\pm0.5)R$ (dotted curve). (e): longitudinal variation over range $0.5 \le X/D \le 10D$. Half-width of Gaussian profile also shown ($-\cdot-$) as Eq. (6). (a) $0.5D$. (b) $1D$. (c) $1.5D$. (d) $2D$. (e) Longitudinal variation.

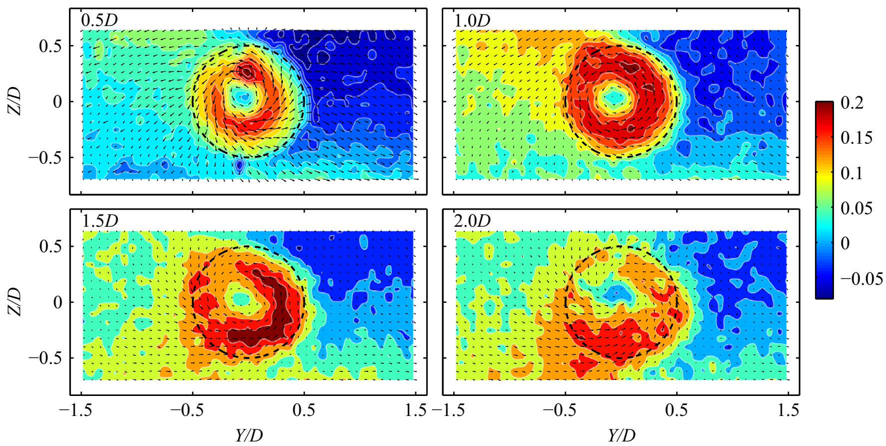

Fig. 10. Velocity components U_y, U_z superposed on contours of azimuthal velocity U_θ in the vertical Y–Z plane at $X=0.5D$, $1D$, $1.5D$ and $2D$ downstream of rotor plane. Obtained from time-varying samples as Fig. 6.

downstream. As the rotating flow field develops, transverse velocities of up to 10% of the streamwise flow occur near the bed (e.g. $Z=-0.62D$, $0.12h$ above bed, over $-1.5D<Y<0$ at $X=2D$). The induced angular velocity of the wake is defined by the mean azimuthal velocity as $\omega(r)=U_\theta(r)/r$. Here the mean azimuthal velocity at radius r is given by

$$U_\theta=\frac{\Gamma}{2\pi r}. \tag{8}$$

This follows from consideration of the circulation, Γ, within radius r

$$\Gamma(r)=\oint_0^{2\pi} U_\theta(r,\theta) r\, d\theta=\int_A \Omega(r,\theta)\, dA, \tag{9}$$

where vorticity is given by

$$\Omega(r,\theta)=\frac{U_\theta}{r}+\frac{dU_\theta}{dr}-\frac{1}{r}\frac{dU_\theta}{d\theta}. \tag{10}$$

At $0.5D$ and $1D$ vorticity is positive within the wake due to anticlockwise rotation whereas vorticity is negative around the circumference of the wake caused by entrainment of the surrounding flow (Fig. 11). The intensity of positive vorticity within the wake area decays rapidly to be similar to the surrounding flow by $2D$ downstream. Negative vorticity along the

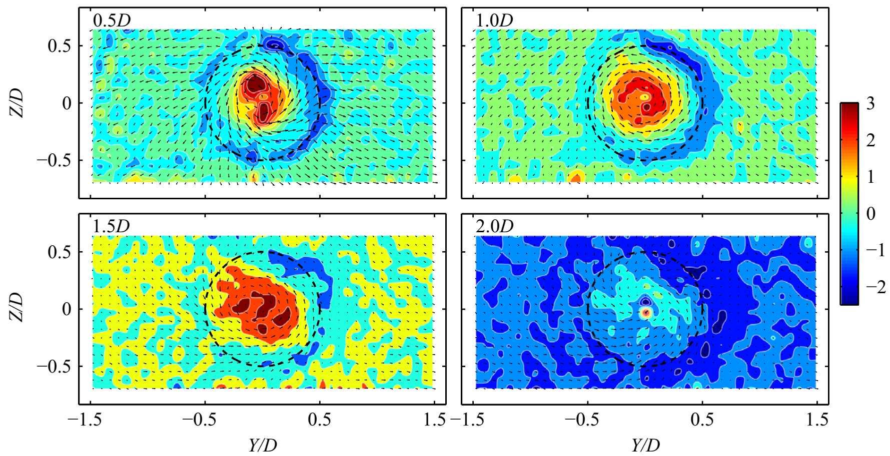

Fig. 11. Vorticity (Ω, as Eq. (10)) in vertical Y–Z plane at sections $X = 0.5D, 1D, 1.5D$ and $2D$ downstream of rotor. Obtained from time-varying samples as Fig. 6.

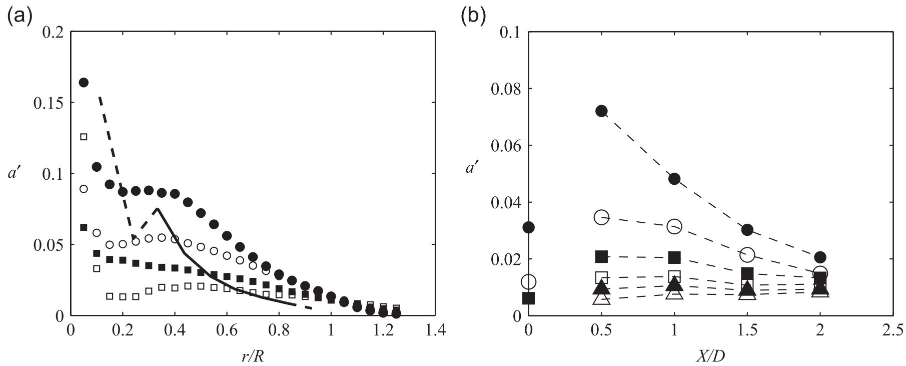

Fig. 12. Tangential induction factor. (a) Radial variation at $0.5D$ (●), $1D$ (○), $1.5D$ (■), $2D$ (□) downstream and by BEMT at rotor plane (–). (b) Streamwise variation at $0.50R$ (●), $0.75R$ (○), $0.9R$ (■), $1.0R$ (□), $1.05R$ (▲) and $1.1R$ (Δ) and by BEMT at rotor plane.

wake circumference reduces in intensity as the azimuthal velocity of the surrounding flow increases. Integration of vorticity over the rectangular measurement region shows that circulation is effectively constant, at close to 0.01 of circulation at the blade tip, and vorticity is conserved.

A tangential induction factor (denoted $a'(r) = \omega(r)/\omega_m - 1$ in blade element momentum theory) is typically employed to represent angular velocity of the flow relative to the angular speed of the rotor ($\omega_m = U_0\beta/R$). The induced rotation as described by this standard parameter varies radially and with distance downstream as shown in Fig. 12. For the four transverse planes considered, rotation is observed for $r > R$. A standard blade element momentum theory calculation of tangential induction factor (for which a' represents flow at the rotor plane and, for unbounded conditions, $2a'$ represents the wake) predicts the trend of radial variation observed at $X = 0.5D$. However, the magnitude of the induced rotation is underpredicted, particularly as r approaches R, perhaps due to sensitivity to lift, drag and angle of incidence. Over the interval $0.5D$ to $2D$ there is rapid decay of rotation within the rotor plane ($r < R$) but induced rotation remains nearly constant ($a' \sim 0.01$) outside the rotor plane.

5. Wake turbulence

The far wake has been shown to exhibit classical self-similar behaviour of mean velocity for shallow turbulent jets and wakes. The free shear layers originating from the rotor circumference have spread across the centreline. The longitudinal turbulence intensity (u'_x/U_0) is shown for the transverse $y-z$ planes downstream of the rotor plane in Fig. 13. Immediately downstream, at $X = 0.5D$, a narrow band of turbulence from tip vortices is observed and there is a region of turbulence downstream of the tower. This tower wake is not observed further downstream. At $1D$ and $1.5D$ a shear layer is clearly defined with turbulence intensity in the wake core comparable to that of the ambient flow and a band of turbulence intensity of 25–30% just outside the rotor radius. The region of greater turbulence intensity has approached, but not reached, the axial centreline by $X = 2D$ consistent with the shear layer width at this distance. Transverse and vertical profiles of turbulence intensity are shown in Fig. 14. The difference between near wake profiles ($x < 6D$) and far wake ($x \geq 8D$) is

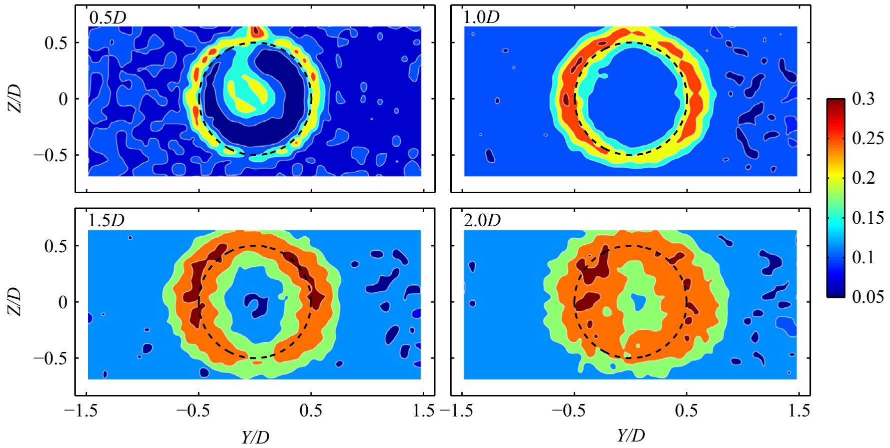

Fig. 13. Turbulence intensity at four planes downstream of rotor. Obtained from time-varying samples as Fig. 6.

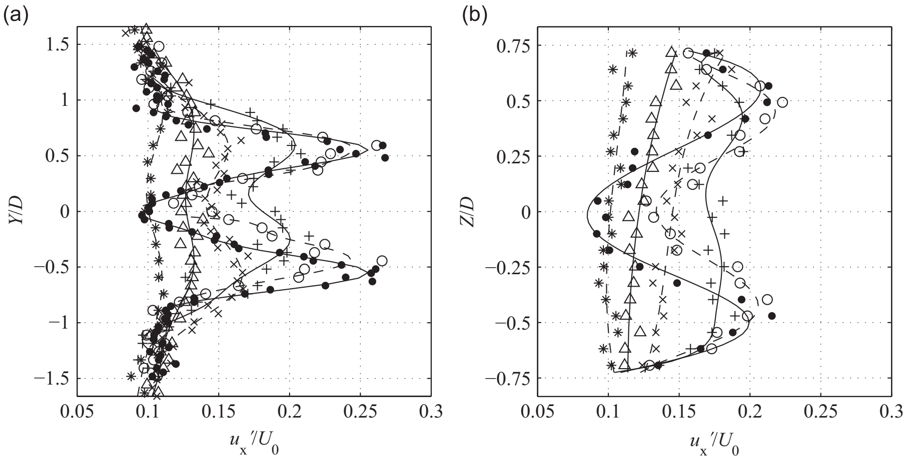

Fig. 14. Transverse and vertical profiles of turbulence intensity at $X=1.5D$ (●), $2D$ (○), $4D$ (+), $6D$ (×), $8D$ (Δ) and $12D$ (✻) corresponding to velocity profiles of Fig. 3. Curves indicate trend only.

apparent as is the difference between transverse and vertical profiles in the far wake. Vertical profiles are almost uniform but transverse variation is still apparent at $X=12D$ with maximum turbulence intensity observed close to the maxima of velocity gradient as used to define wake width.

6. Conclusions

The mean wake of a three-bladed tidal stream rotor has been measured in a wide flume with minimal blockage and diameter of 60% of the water depth. The rotor was operated at close to maximum power coefficient and generated a thrust coefficient representative of a full scale turbine. The mean near wake is characterised by free shear layers originating from the rotor tip circumference and with linear expansion of thickness with downstream distance. The rate of expansion is typical of a plane shear layer vertically and 1.5 times that horizontally. The radius of the shear layer centreline remains similar to the rotor radius until the wakes merge at about 2.5 rotor diameters downstream. A self-similar two-dimensional wake develops from about eight diameters downstream with a virtual origin at 2.0 diameters downstream of the rotor plane. The spreading rate is somewhat less than that measured for solid bodies. The mean velocity profiles, rotation and vorticity are similar to those previously measured for wind and marine turbines in the near wake. However longitudinal circulation in the transverse plane was measured to be close to 1% of the circulation at the blade tip within two diameters downstream, the extent of detailed measurement. The standard blade element momentum theory that is widely used for rotor design characterises velocity at the rotor plane by axial and tangential induction factors. While this flow representation is highly idealised it is interesting to observe that the axial induction factor corresponds to velocity deficits at 0.4–0.8 radii from the centreline across the near wake while the tangential induction factor at the rotor plane corresponds to velocities at 0.4–0.6 radii between 1–2 diameters downstream, indicating some correspondence with the real flow. The important characterisation of the far wake in a shallow channel as a two-dimensional self-similar form is defined by two parameters defining the centreline velocity deficit and transverse velocity variation. These are likely to be insensitive to Reynolds number in turbulent conditions although this should be assessed for full scale conditions. This self-similar form for the far wake is a useful categorisation for the assessment of wake interaction within turbine arrays.

Acknowledgements

This study was supported by the Performance of Arrays of Wave and Tidal Array Systems (PerAWaT) project commissioned by the Energy Technologies Institute (ETI) and by EPSRC Grant EP/J010235/1 (X-MED). The thrust curve of the small-scale rotor employed in these experiments is based on the performance of a generic full-scale rotor provided to the PerAWaT consortium by Tidal Generation Ltd. Technical discussions with members of the PerAWaT consortium are gratefully acknowledged.

References

Afgan, I., McNaughton, J., Rolfo, S., Apsley, D., Stallard, T., Stansby, P., 2013. Turbulent flow and loading on a tidal stream turbine by LES and RANS. International Journal of Heat and Fluid Flow 43, 96–108.

Batten, W., Bahaj, A., Molland, A., Chaplin, J., 2008. The prediction of the hydrodynamic performance of marine current turbines. Renewable Energy 33, 1085–1096.

Bossanyi, E., 2009. Tidal Bladed—Theory Manual. Technical Report. 282/BR/009, Garrad Hassan and Partners Ltd.

Brown, G., Roshko, A., 1974. Density effects and large structure in mixing layers. Journal of Fluid Mechanics 64, 775–816.

Brown, R., 2009. Design and Construction of a Dynamometer System for Testing an Array of Wave Energy Point Absorbers M.Phil. Thesis. University of Manchester.

Chamorro, L., Hill, C., Morton, S., Ellis, C., Arndt, R., Sotiropoulos, F., 2013. On the interaction between a turbulent open channel flow and an axial-flow turbine. Journal of Fluid Mechanics 716, 658–670.

Hassan, U., 1993. A Wind Tunnel Investigation of the Wake Structure Within Small Wind turbine Farms. Technical Report. WN 5113, ETSU.

Högstrom, U., Asimakopoulos, D., Kambezidis, H., Helmis, C., Smedman, A., 1988. A field study of the wake behind a 2 MW wind turbine. Atmospheric Environment 22, 803–820.

Hu, H., Yang, Z., Sarkar, P., 2011. Dynamic wind loads and wake characteristics of a wind turbine model in an atmospheric boundary layer wind. Experiments in Fluids 52, 1277–1294.

Hussain, A., Zedan, M., 1978. Effects of the initial condition on the axisymmetric free shear layer: effects of momentum thickness. Physics of Fluids 21, 1100–1112.

Lissamen, P., 1983. Low Reynolds number airfoils. Annual Review of Fluid Mechanics 15, 223–239.

Maganga, F., Germain, G., King, J., Pinon, G., Rivoalen, E., 2010. Experimental characterization of flow effects on marine current behaviour and on its wake properties. IET Renewable Power Generation 4, 498–509.

Magnusson, M., Smedman, A., 1999. Air flow behind wind turbines. Journal of Wind Engineering & Industrial Aerodynamics. 80, 169–189.

McNaughton, J., Afgan, I., Apsley, D., Rolfo, S., Stallard, T., Stansby, P., 2014. A simple sliding-mesh interface procedure and its application to the simulation of a tidal-stream turbine. International Journal for Numerical Methods in Fluids 74, 250–269.

Miley, S., 1982. A Catalog of Low Reynolds Number Airfoil Data for Wind Turbine Applications. Technical Report. DE82-021712, NTIS.

Myers, L., Bahaj, A., 2010. Experimental analysis of the flow field around horizontal axis tidal turbines by use of scale mesh disk rotor simulators. Ocean Engineering 37, 218–227.

Nezu, I., Nakagawa, H., 1993. Turbulence in Open Channel Flows. IAHR/AIRH. A.A.Balkema, Rotterdam-Brookfield.

Nortek, 2006. Vectrino+ User Manual. Technical Report, NORTEK.

Pope, S.B., 2000. Turbulent Flows. Cambridge University Press.

Stallard, T., Collings, T., Feng, T., Whelan, J., 2013. Interactions between tidal turbine wakes: experimental study of a group of 3-bladed rotors. Philosophical Transactions of the Royal Society A 371. 2012.0159.

Stansby, P.-K., 2003. A mixing length model for shallow turbulent wakes. Journal of Fluid Mechanics 495, 369–384.

Thomson, J., Polagye, B., Durgesh, V., Richmond, M., 2012. Measurements of turbulence at two tidal energy sites in Puget Sound, WA. IEEE Journal of Oceanic Engineering 37, 363374.

Vermeer, L., Sorensen, J., Crespo, A., 2003. Wind turbine wake aerodynamics. Progress in Aerospace Sciences 39, 467–510.

Way, S., Collier, W., 2–5 September 2013. Full-scale validation study of a numerical tool for the prediction of the loading and hydrodynamic performance of axial flow tidal turbines. In: Frigaard, P. (Ed.), Proceedings of Tenth European Wave and Tidal Energy Conference.

Weller, S., Stallard, T., Stansby, P., 2010. Experimental measurements of irregular wave interaction factors in closely spaced arrays. IET Renewable Power Generation 4, 628–637.

Whelan, J., Stallard, T., 5–9 September 2011. Arguments for modifying the geometry of a scale model rotor. In: Bahaj, A. (Ed.), Proceedings of the Eighth European Wave and Tidal Energy Conference. p. on CD. Paper No. 50.

Wu, Y., Porte-Agel, F., 2011. Large-eddy simulation of wind-turbine wakes: evaluation of turbine parameterizations. Boundary-Layer Meteorology 132, 129–149.

Zhang, W., Markfort, C., Porte-Agel, F., 2012. Near-wake flow structure downwind of a wind turbine in a turbulent boundary layer. Experiments in Fluids 52, 1219–1235.